

# Graphene oxide/multi-walled carbon nanotubes/gold nanoparticle hybridfunctionalized disposable screen-printed carbon electrode to determine Cd(II) and Pb(II) in soil

Hui Wang<sup>1,4</sup>, Yuan Yin<sup>1</sup>, Guo Zhao<sup>1</sup>, Fernando Bienvenido<sup>2</sup>, Isabel M. Flores-Parrad<sup>2</sup>, Zhiqiang Wang<sup>3</sup>, Gang Liu<sup>1\*</sup>

(1. Key Laboratory of Modern Precision Agriculture System Integration Research, Ministry of Education and Key Laboratory of Agricultural Information Acquisition Technology, Ministry of Agriculture, China Agricultural University, Beijing 100083, China;

2. Department of Informatics, University of Almeria, Almeria, Spain;

3. College of Computer Science and Technology, Shandong University of Technology, Zibo 255049, China;

4. Research Institute of Wood Industry, Chinese Academy of Forestry, Beijing 100091, China)

**Abstract:** Cadmium (Cd) and lead (Pb) in soil or water environment cause the ecological destruction and environmental deterioration when their contents exceed the natural background values. To trace the concentrations of Cd(II) and Pb(II), a sensitive and selective electrode was developed using disposable screen-printed carbon electrode (SPE) immobilized with a composite film of reduced graphene oxide/carboxylation multi-walled carbon nanotubes/gold nanoparticle hybrid (RGO-MWNT-AuNP) through  $\pi$ - $\pi$  bind. This highly conductive nano-composite layer, "RGO-MWNT-AuNP," was characterized by scanning electron microscopy, UV-visible spectrometer, cyclic voltammetry, and electrochemical impedance spectroscopy. Square wave stripping voltammetry was applied to RGO-MWNT-AuNP/SPE to electroplate bismuth film and monitor the Cd(II) and Pb(II) simultaneously. To obtain high current responses, the detecting parameters were optimized. Under optimized conditions, the current responses showed a linear relationship with the concentrations of Cd(II) and Pb(II) in the range from 1.0 to 80.0  $\mu\text{g/L}$  with a lower detection limit of 0.7  $\mu\text{g/L}$  and 0.3  $\mu\text{g/L}$  ( $S/N = 3$ ), respectively. Finally, the prepared electrode was further employed to detect Cd(II) and Pb(II) in soil samples with good results.

**Keywords:** electrochemical electrode, heavy metal contamination, screen-printed carbon electrode, graphene, gold nanoparticle, lead, cadmium, multi-walled carbon nanotube

**DOI:** 10.25165/j.ijabe.20191203.4300

**Citation:** Wang H, Yin Y, Zhao G, Bienvenido F, Flores-Parrad I M, Wang Z Q, et al. Graphene oxide/multi-walled carbon nanotubes/gold nanoparticle hybridfunctionalized disposable screen-printed carbon electrode to determine Cd(II) and Pb(II) in soil. Int J Agric & Biol Eng, 2019; 12(3): 194–200.

## 1 Introduction

Heavy metals, including mercury (Hg), cadmium (Cd), lead (Pb), chromium (Cr), Copper (Cu) and Arsenic (As)<sup>[1]</sup>, are widely distributed in natural environment, which have serious hazards to human health and proved by many researches. Lead ion (Pb(II)) and cadmium ion (Cd(II)), which are two of the most common contaminants, attracted stronger interest in China due to their vast emissions and persistent environmental pollution<sup>[2,3]</sup>. In the agricultural environment, Pb(II) and Cd(II) in soil or water are

mainly derived from wastewater discharge, vehicle emissions, lead-acid batteries, fertilizers, mining and industrial wastes<sup>[1,4]</sup>. According to a nationwide survey conducted by the Chinese government which evaluated 6.3 million km<sup>2</sup> of various land from 2005 to 2013, half of these land was suffering contamination from heavy metals especially lead and cadmium in varying degrees, caused a severe threat to food safety, ecological environment, and sustainable agricultural development. These two heavy metals in farmland soil are easily absorbed by crops and vegetables, which can be entered and enriched in human body through multiple absorption ingestion and dermal contact. Pb(II) and Cd(II) that binded with enzymes, nucleic acids and structural proteins will interfere, impact and destruct the body's normal function<sup>[5]</sup>, and they can further cause server diseases such as pneumonitis, lung cancer, osteomalacia, anemia, encephalopathy<sup>[6]</sup>. To assess the levels of Pb(II) and Cd(II) in soil, a cheap and convenient analytical tool is urgent to develop for heavy metal ions determination. Currently, many methods have been exploited and applied in testing organizations during the past decades, including atomic absorption spectrometry<sup>[7]</sup>, inductively coupled plasma mass spectrometry<sup>[8,9]</sup>, capillary electrophoresis<sup>[10]</sup>, X-ray fluorescence spectrometry<sup>[11]</sup>, and quantum dot<sup>[12]</sup>. Most of these techniques have high sensitivity and selectivity, but they required bulk and expensive instrument, sophisticated operation and

**Received date:** 2018-04-06 **Accepted date:** 2019-03-11

**Biographies:** Hui Wang, PhD, Assistant Research Fellow, research interests: electrochemical sensor and biosensor, Email: wanghui\_lunwen@163.com, wanghuilunwen@cau.edu.cn; Yuan Yin, PhD candidate, research interests: electrochemical sensor, Email: 1144729812@qq.com; Guo Zhao, PhD candidate, research interests: electrochemical sensor and pattern recognition, Email: 1252624780@qq.com; Fernando Bienvenido, PhD, research interests: image processing and pattern recognition, Email: fbienve@ual.es; Isabel M. Flores-Parrad, PhD, research interests: GIS and satellite images, Email: iflores@ual.es; Zhiqiang Wang, PhD, Professor, research interests: pattern recognition and electrochemical sensor, Email: 147551982@qq.com.

\*Corresponding author: Liu Gang, PhD, Professor, research interests: electrochemical sensor and biosensor. College of Information and Electrical Engineering, China Agricultural University, Beijing 100083, China. Tel: +86-10-62736741, Email: pac@cau.edu.cn.

complex pretreatment that make them difficult to detect heavy metal ions on-site. Electrochemical method<sup>[13]</sup> has gained a widespread attention in recent years because of its simple operation, small device and inexpensive electrodes. Carbon paste electrode and glassy carbon electrode are the common working electrodes in electrochemical sensing, but their price is relatively higher than disposable screen-printed electrode (SPE)<sup>[14]</sup>. Besides, SPE integrated three electrodes (a working electrode, a reference electrode, and a counter electrode) on a substrate, owns some significant advantages that can be produced in enormous quantities. However, bare SPE has many drawbacks including low sensitivity and poor selectivity, which makes it hard to trace the super-low level of Cd(II) and Pb(II).

Several new materials, such as nano materials<sup>[14]</sup>, conductive polymer<sup>[15]</sup>, ionic liquids<sup>[16]</sup> and biologic material<sup>[17]</sup>, have been applied in the field of electrochemistry to improve the detecting performance. Biologic materials containing proteins, nucleic acids and cells can bind Cd(II) and Pb(II) with high affinity and specificity, but they are more susceptible to the environment which limits their application. Nanomaterials like graphene<sup>[18]</sup> and carbon nanotubes<sup>[19]</sup> have many unusual characters such as physicochemical, mechanical, excellent electrical, optical and thermal conductivity, which makes them been applied in many fields. Some researchers tried to combine graphene and carbon nanotubes. They found that carbon nanotubes can connect with graphene to bridge the defects for electron transfer, and these hybrid materials have a unique synergistic effect of graphene and carbon nanotubes<sup>[20,21]</sup>. Graphene oxide<sup>[22]</sup> is an oxygenated derivative of graphene which has excellent hydrophobicity, which makes it easily form a homogeneous liquid with water to provide active sites for the interaction with other aromatic compounds. Gold nanoparticles (AuNP) have many special physical and chemical properties including large specific surface area, high surface energy, quantum dimension effect and macroscopic quantum tunneling effect.

Screen-printed carbon electrode (SPE) is a low cost, small-size, portable and easy-to-use electrode, which have been modified with different chemical materials and biomaterials to improve the specificity and sensitivity. This study synthesized a nano-composite material using graphene oxide, multi-wall carbon nanotube and gold nano particles, which was used to modify a disposable SPE to overcome the poor detecting performance. After GO reduced by cyclic voltammetry, RGO-MWNT-AuNP/SPE is plated a bismuth film in situ that obtains the current signal of Cd(II) and Pb(II) at the same time. The properties of SPE before and after each modification were investigated by some methods. After optimized the electroanalytical parameters, the modified SPE was employed to detect the Cd(II) and Pb(II) using square wave stripping voltammetry.

## 2 Materials and methods

### 2.1 Chemicals and reagents

Three standard solutions of Bi(III), Cd(II) and Pd(II) (1000 mg/L) were offered by National Standard Reference Materials Center (Beijing, China), which were diluted as required before use. Graphene oxide and multi-walled carbon nanotube were bought from Xianfeng Nano-Materials Technology Co., Ltd. (Nanjing, China). HAuCl<sub>4</sub> were purchased from Aldrich (Sigma-Aldrich US). Potassium ferricyanide was obtained from Shanghai Chemical Reagent Co. (Shanghai, China). Sodium phosphate

buffer solution was employed as supporting electrolyte to reduce GO-MWNT-GNP hybrid. Sodium acetate buffer solution was took as the supporting electrolyte for the Cd(II) and Pb(II) determination. The rest of chemicals that not mentioned here were of analytical reagent grade and were used as received. All solutions were prepared using Milli-Q purified water (>18.2 MΩ/cm<sup>3</sup>).

### 2.2 Instrument

All electrochemical measurements were conducted using CHI 660D electrochemical workstation, which were purchased from the CHI Instrument Company (Shanghai, China). Three electrodes were integrated on the same substrate (Bi/RGO-MWNT-AuNP/SPE as the working electrode, printed Ag electrode as the reference electrode and printed carbon electrode as the auxiliary electrode). A PHS-3C digital pH-meter was purchased from Shanghai Instrument Scientific Instrument Co., Ltd, China. UV-vis experiments were measured using a UV-2100S spectrophotometer (Shimadzu). The images of scanning electron microscopy (SEM) were achieved by a field-emission scanning electron microscope JEOLJEM-2011 device. All measurements were carried out at room temperature.

### 2.3 Synthesis of GO-MWNT-GNP and AuNP

The GO-MWNT hybrid was synthesized using the protocol reported in previous report<sup>[23]</sup>. Briefly, MWNT were refluxed with mixture of concentrated HNO<sub>3</sub> and concentrated H<sub>2</sub>SO<sub>4</sub> (V/V=1:3) for 6 h. The carboxylation of MWNT(c-MWNT) was filtered and rinsed with sufficient Milli-Q purified until neutral pH was achieved. Additionally, the c-MWNT were dried at high temperature in a vacuum oven. 1 mg c-MWNTs were dispersed in 1 mL Milli-Q purified water to form a homogeneous solution, and then the dispersed solution was mixed with 1 mL GO (1 mg/mL) suspension, which was further sonicated for 0.5 h to form a uniform GO-MWNT complexes.

The AuNP were synthesized using citrated reduction method<sup>[24]</sup>. Before the experiment, all glasswares were immersed in aqua regia and rinsed with sufficient water to remove the potential artificial nucleation sites. 50 mL of 1 mmol/L tetrachloroaurate trihydrate solution was boiled with vigorous stirring until the temperature reached 97 °C, and 1.5% trisodium citrate was then added to the boiling solution as soon as possible. The mixed solution stops stirring when its color turns brilliant red.

### 2.4 Electrode preparation

The GO-MWNT-AuNP hybrid was prepared by mixing 20 μL GO-MWNT, 20 μL AuNP, 50 μL water and 10 μL ethyl alcohol. 4 μL GO-MWNT-AuNP hybrid was coated on the working electrode surface, which was dried in air for 30 min to obtain GO-MWNT-AuNP/SPE. After that, GO-MWNT-AuNP/SPE was immersed in 0.1 mol/L PBS (pH 7.0) and reduced the GO to gain RGO-MWNT-AuNP/SPE through cyclic voltammetry with scan rate 20 mV/s as shown in Figure 1.

### 2.5 Measurement procedures

For the Cd(II) and Pb(II) determination, the measurements using the square wave anodic stripping voltammetry (SWASV) were performed in 0.1 mol/L sodium phosphate buffer solution with the presence of 1 mg/L Bi(III). Before the analysis, three electrodes were immersed in the extract of soil samples, and a negative potential (-1.4 V) was applied to the working electrode with stirring in the test solution during the deposition steps. After a 20 s equilibration period, the potential scan of SWASV was scanned from -1.4 V to +0.0 V.

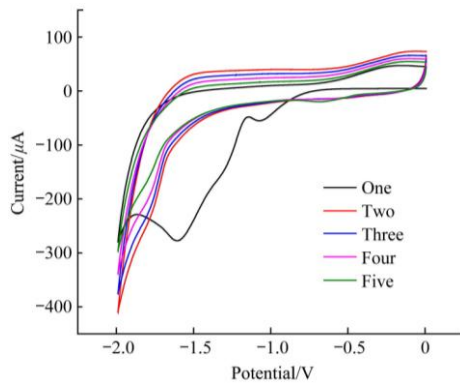


Figure 1 Cyclic voltammograms of GO-MWNT-AuNP/SPE in 0.1 mol/L PBS (pH 7.0) for 5 cycles. Scan rate: 20 mV/s

### 3 Results and discussion

#### 3.1 Characterization of RGO-MWNT-AuNP/SPE

The microstructure of the working electrode surface was investigated via the scanning electron microscope (SEM). Figure 2 shows the SEM images of SPE, RGO-MWNT/SPE, and

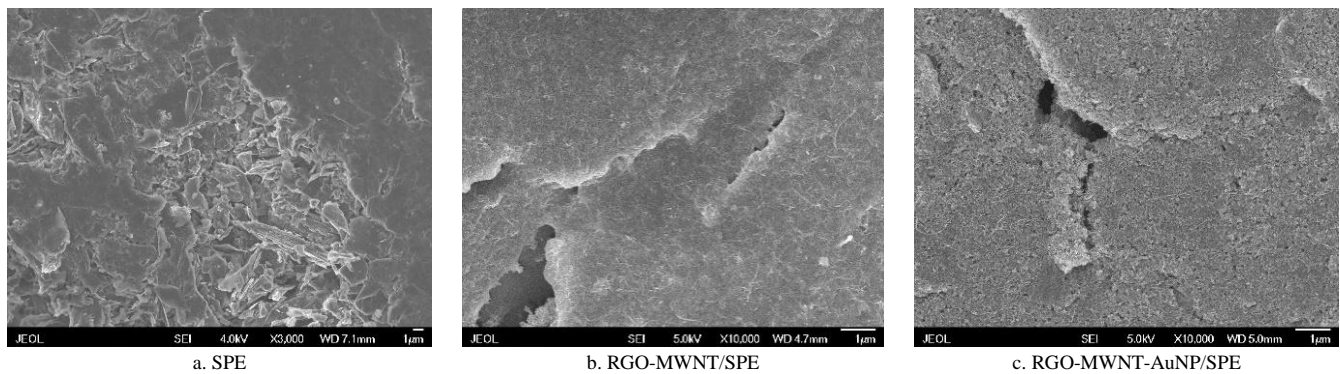


Figure 2 SEM images of SPE, (b) RGO-MWNT/SPE and (c) RGO-MWNT-AuNP/SPE

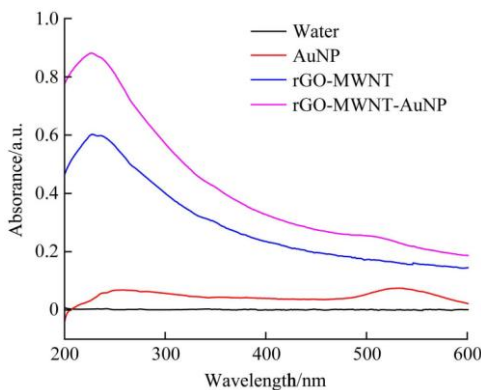


Figure 3 UV-vis absorption spectra of water (black line), AuNP (red line), GO-MWNT (blue line) and GO-MWNT-AuNP (purple line)

#### 3.2 CV and EIS characterization

Figure 4 shows the CV responses of bare SPE, RGO-MWNT/SPE and RGO-MWNT-AuNP/SPE in a mixture solution of 5 mmol/L  $[\text{Fe}(\text{CN})_6]^{3-/4-}$  and 0.1 mol/L KCl. The CV curve of SPE displayed a pair of redox peak with the peak-to-peak separation of 280 mV, and the peak current is about 70  $\mu\text{A}$ . While RGO-MWNT was coated on SPE through the  $\pi$ - $\pi$  bond, the redox peak current was enhanced, and the peak-to-peak separation was decreased due to the high conductivity and large specific surface area of RGO and MWNT. After RGO-MWNT mixed with AuNP was modified on SPE, the peak currents of RGO-MWNT-

RGO-MWNT-AuNP/SPE. The morphology of SPE in Figure 2(a) exhibited some large irregular stones gaps and graphite blocks. After SPE functionalized with RGO-MWNT hybrid, RGO and MWNT were homogeneously distributed on the working electrode surface, which owns a large specific surface area due to the special structure of RGO and MWNT. From the SEM image of RGO-MWNT-AuNP/SPE, there were too many tiny gaps distributed on the working surface that can provide large interface compared to RGO-MWNT, which was contributed to AuNP.

UV-vis spectroscopy was employed to analyze the dispersed solution of different materials. From the Figure 3, it was obvious that the UV-vis spectrum of AuNP in water displayed two absorption bands at 250 nm and 540 nm, and the absorption band of GO-MWNT was located at 240 nm. When these two materials were mixed, the UV-vis spectrum of this new hybrid shows a small absorption band at 540 nm and a high absorption band at 250 nm. The results seem like the sum of the absorption of AuNP and GO-MWNT, indicating that these two material form a homogeneous solution.

AuNP/SPE increased and the peak-to-peak separation decreased obviously, demonstrated that nano-composite membrane has specific surface area and excellent conductivity that can improve the charge transfer.

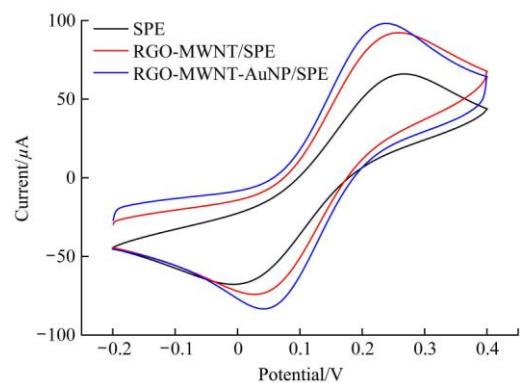


Figure 4 Cyclic voltammograms of bare SPE, RGO-MWNT/SPE and RGO-MWNT-AuNP/SPE in 5.0 mmol/L  $[\text{Fe}(\text{CN})_6]^{3-/4-}$  and 0.1 mol/L KCl solution at a scan rate of 50 mV/s

EIS was a useful method to characterize the impedance changes of SPE before and after modification, which was consisted by a semicircle part at higher frequencies and a linear part at the lower frequencies that presented the electron transfer resistance ( $R_{\text{et}}$ ) and the diffusion process, respectively. In Figure 5, the  $R_{\text{et}}$  value of SPE was about 2100  $\Omega$ . After RGO-MWNT was immobilized on SPE, the conductivity between RGO-MWNT/SPE and

electrolyte was enhanced, and the  $R_{ct}$  value decreased to 1500  $\Omega$ . Similarly,  $R_{ct}$  value of the RGO-MWNT-AuNP/SPE was about 1100  $\Omega$  due to the synergistic effect of AuNP and RGO-MWNT. The results were in agreement with the conclusion obtained from the CV.

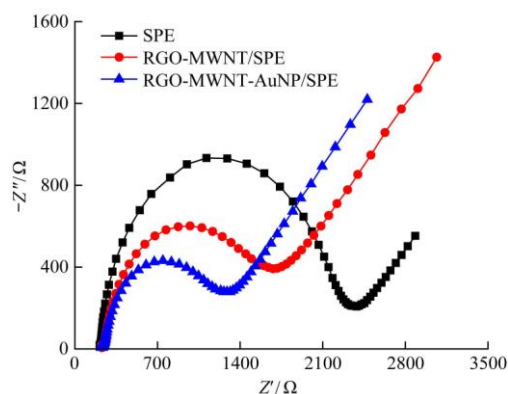


Figure 5 Electrochemical impedance spectra of bare SPE, RGO-MWNT/SPE and RGO-MWNT-AuNP/SPE with the frequencies from 1 to  $10^5$  Hz in 5 mmol/L  $[\text{Fe}(\text{CN})_6]^{3-/4-}$  and 0.1 mol/L KCl

The potential window of RGO-MWNT-AuNP/SPE before and after electroplating Bi film was tested in Figure 6. The RGO-MWNT-AuNP/SPE without bismuth film had a narrow potential window, which was greater  $-1.2$  V. If the potential was lower than  $-1.2$  V, the current response was increased significantly because of the hydrogen evolution occurring on the electrode surface. After reducing a Bi film, Bi/RGO-MWNT-AuNP/SPE can obtain a relative negative hydrogen over voltage potential about  $-1.6$  V, which was ascribed to the special crystal plane structure of bismuth.

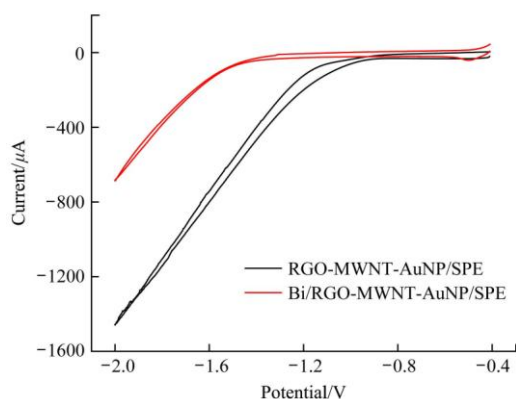


Figure 6 Cyclic voltammograms of RGO-MWNT-AuNP/SPE and Bi/RGO-MWNT-AuNP/SPE in 0.1 mol/L acetate buffer solution

Figure 7 shows the SWASV responses of Bi/SPE, Bi/RGO-MWNT/SPE, and Bi/RGO-MWNT-AuNP/SPE, which were used to detect 20  $\mu\text{g/L}$  Cd(II) and 20  $\mu\text{g/L}$  Pb(II) in 0.1 mol/L acetate buffer solution. Two reductive peak currents for the Cd(II) and Pb(II) determination was observed at  $-1.1$  V and  $-0.85$  V on the SPE. The change of reductive potentials was mainly because the reference electrode of Ag/AgCl was replaced by the Ag electrode, and the electrode potentials of these two reference electrode were different. Bi/RGO-MWNT/SPE and Bi/RGO-MWNT-AuNP/SPE exhibited much higher current responses toward Cd(II) and Pb(II) determination in comparison to SPE's. The reason was that nano-composite film of RGO-MWNT and RGO-MWNT-AuNP

had a high specific surface area that provided more binding sites.

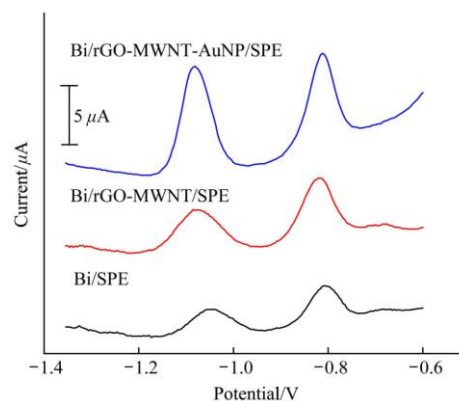


Figure 7 SWASV responses of (a) Bi/SPE, (b) Bi/RGO-MWNT/SPE and (c) Bi/RGO-MWNT-AuNP/SPE in 0.1 mol/L acetate buffer solution with 20  $\mu\text{g/L}$  Cd(II) and 20  $\mu\text{g/L}$  Pb(II)

### 3.3 Optimization

To improve the current response for Pb(II) and Cd(II), several critical detecting parameters of Bi/RGO-MWNT-AuNP/SPE were optimized in 0.1 mol/L sodium acetate buffer solution, which contained 50  $\mu\text{g/L}$  Cd(II) and 50  $\mu\text{g/L}$  Pb(II).

Bi film decorated on electrodes in-site is used to improve the sensitivity for the detection of Cd(II) and Pb(II) because Bi(III) can form a complex with Cd(II) and Pb(II) that makes their concentration reduced efficiently. Figure 8a displays the current response of Cd(II) and Pb(II) associated with the Bi(III) concentration. It was obvious that the current responses of Cd(II) and Pb(II) were of positive relevance with Bi(III) concentrations ranging from 0 to 1 mg/L. The adequate Bi(III) with Cd(II) and Pb(II) can form a complex to decrease the activation energy for cathodic preconcentration. When the Bi(III) concentration was higher than 1 mg/L, the current responses of Cd(II) and Pb(II) decreased. Thus, 1 mg/L of Bi(III) was chosen in the experiments.

Figure 8b shows that the current responses of Cd(II) and Pb(II) were affected by the pH of the sodium acetate buffer solution. Different pH in the range from 3.5 to 5.5 was investigated for the Cd(II) and Pb(II) detection. The highest current responses of Cd(II) and Pb(II) were located at pH4.5. The reason was that hydrogen generated at excessively acidic circumstances on electrode surface can damage the quality of the bismuth film. In contrast, the current responses remained low due to the hydrolysis of Bi(III) at higher pH. Hence, pH4.5 was used throughout the experiments.

Figure 8c shows the deposition potential associated with the current response of Cd(II) and Pb(II). The current responses of Cd(II) and Pb(II) were enhanced with the deposition potential ranging from  $-1.2$  to  $-1.4$  V, and then decreased remarkably when the deposition potential was higher than  $-1.4$  V, which was attributed to the hydrogen evolution reaction that prevented the deposition of Cd(II) and Pb(II) on the surface. Therefore,  $-1.4$  V was chosen as the optimized deposition potential.

Figure 8d shows that the current response was affected by the deposition time. The peak currents increased with the deposition time from 60 to 420 s. However, the peak currents increased gradually when the deposition time exceeded 300 s. With the consideration of the rapid detection, 300 s was selected as the optimized deposition time.

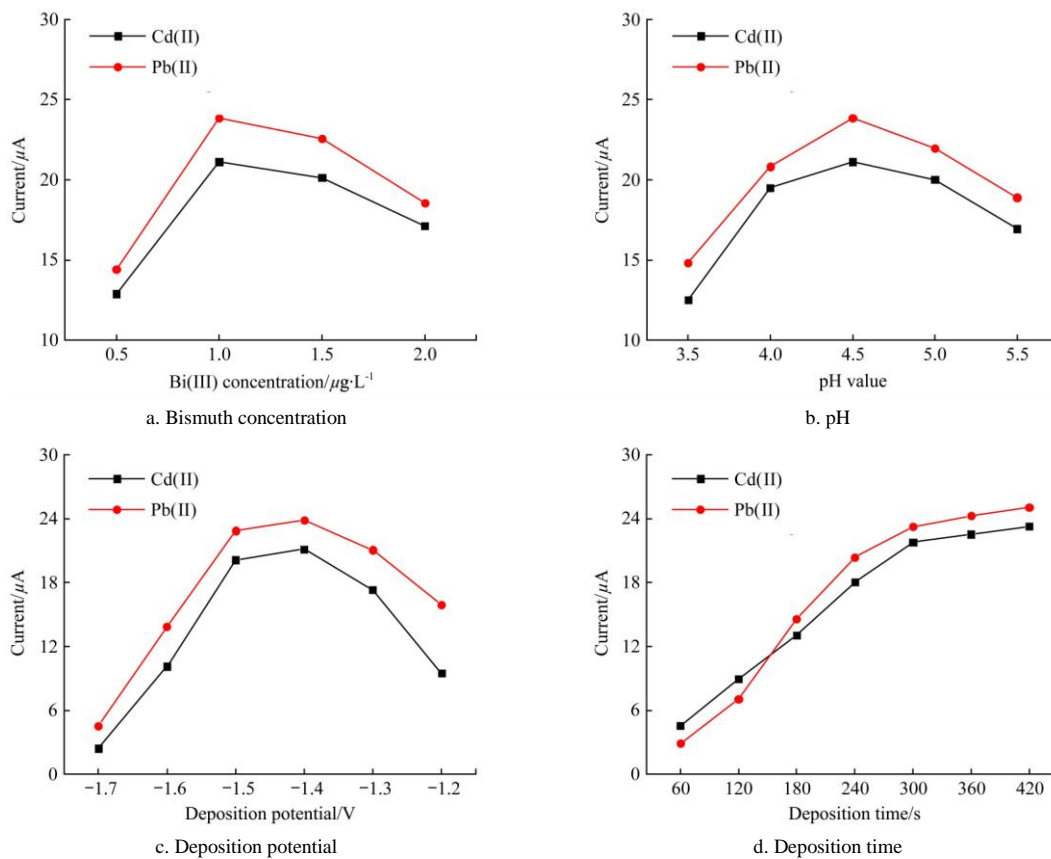


Figure 8 SWASV responses for 50 µg/L Cd(II) and 50 µg/L Pb(II) detection in 0.1 mol/L acetate buffer solution affected by (a) bismuth concentration, (b) pH, (c) deposition potential and (d) deposition time

**3.4 Analytical performance of Bi/RGO-MWNT-AuNP/SPE**

The calibration curves for Cd(II) and Pb(II) determination were performed on the Bi/RGO-MWNT-AuNP/SPE under the optimal conditions. The electrode was immersed in 0.1 mol/L acetate buffer solution (pH 4.5) by adding the standard solution. Figure 9 shows a series of current responses for different concentrations of Cd(II) and Pb(II). It was found that the current responses and the concentrations of Cd(II) and Pb(II) exhibited a linear relation in the range from 1 µg/L to 80 µg/L. The regression equations were:  $I(\mu A) = 0.4413 \times C(\mu g/L) + 0.3001$  and  $I(\mu A) = 0.4893 \times C(\mu g/L) + 0.6285$  with the correlation coefficients

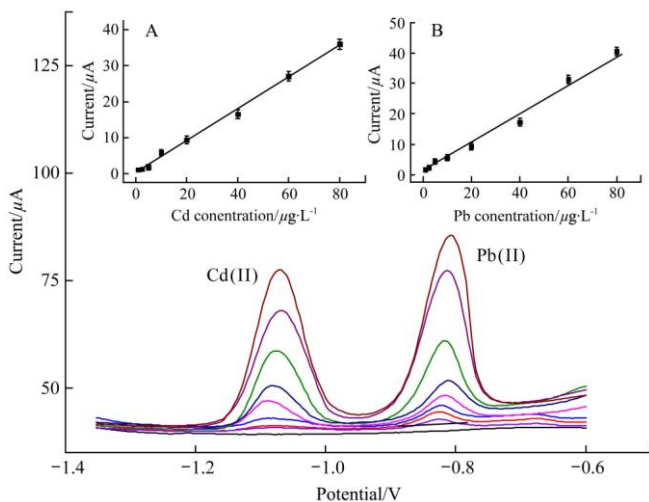


Figure 9 SWASV curves of the Bi/RGO-MWNT-AuNP/SPE to detect different Cd(II) and Pb(II) concentrations ranging from 1 µg/L to 80 µg/L in 0.1 M sodium acetate buffer solution; (A) the calibration curve of Cd(II); (B) The calibration curve of Pb(II)

of 0.99 and 0.99, respectively, where  $I$  was the current response and  $C$  was the concentration of Cd(II) and Pb(II). The limits of detection were 0.7 µg/L and 0.3 µg/L based on three times the standard deviation of the baseline ( $S/N=3$ ).

Compared with heavy metal electrodes reported by other groups, some properties for Cd(II) and Pb(II) detection were summarized in Table 1. It was obvious that the linear range of Bi/RGO-MWNT-AuNP/SPE can reach the performance of the modified glassy carbon electrode, but the low detection limit was much higher than others. The proposed electrode can meet the requirements of the Cd(II) and Pb(II) detection in soil.

**Table 1 Comparison of different electrodes for Cd(II) and Pb(II) detection**

Electrodes	Liner rang/µg L <sup>-1</sup>		Limit of detection /µg L <sup>-1</sup>		References
	Cd(II)	Pb(II)	Cd(II)	Pb(II)	
NF-Bi/NMC/GCE	0.5-80	2-80	0.5	1.5	[25]
Sb/SPAN/EGE	2-70	2-70	0.41	0.20	[26]
Dendritic Bi/GCE	5-50	5-50	0.4	0.1	[27]
BI/MWNT-IL/SPCE	1-60	1-60	0.5	0.12	[28]
BiF/N/IL/G/SPCE	0.1-100	0.1-100	0.06	0.08	[29]
N-GE/nano-CPE	0.001-0.112	0.002-0.2	0.0009	0.001	[30]
Bi/RGO-MWNT-AuNP/SPE	1-80	1-80	0.7	0.3	This work

**3.5 Interference effects**

The performance of anti-interference was an important parameter for the electrochemical electrode. First, the Bi/RGO-MWNT-AuNP/SPE was employed to test the standard solutions of Cd(II) and Pb(II) in Table 2, indicating that Bi/RGO-MWNT-AuNP/SPE had high accuracy. Second, the

modified electrode was also used to test 10  $\mu\text{g/L}$  Cd(II) and 10  $\mu\text{g/L}$  Pb(II) with 10-fold co-existing ions (K(I), Cl(I), Na(I),  $\text{NO}_3(\text{I})$ ,  $\text{CH}_3\text{COO}(\text{I})$ , Mg(II), Ca(II), Co(II), Ni(II),  $\text{SO}_4(\text{II})$ , Fe(III) and Al(III)) under the optimal conditions. The results show that the relative currents of most metal ions were lower than 5%, illustrated that these cations and anions did not interfere with Cd(II) and Pb(II) determination.

**Table 2 Interference between Cd(II) and Pb(II)**

Sample	Standard solution $/\mu\text{g L}^{-1}$		Detection value $/\mu\text{g L}^{-1}$		Relative error /%	
	Cd(II)	Pb(II)	Cd(II)	Pb(II)	Cd(II)	Pb(II)
1	40	0	39.23 $\pm$ 0.83	-	1.93	-
2	0	40	-	40.45 $\pm$ 0.51	-	1.13
3	40	40	40.63 $\pm$ 1.41	40.34 $\pm$ 0.97	1.57	0.85

### 3.6 Analysis of the soil samples

To estimate its application, Bi/RGO-MWNT-AuNP/SPE was employed to sense Cd(II) and Pb(II) in extracting soil solutions. All soil samples were collected from farmland in the suburbs of Beijing city. Before measurement, the soil samples were pretreated to extract Cd(II) and Pb(II)<sup>[31]</sup>. First, soil samples were heating to dry in an oven at a high temperature. Then, the dried samples were ground using a mortar. 1 g of soil was transferred to an extraction bottle and mixed with 0.1 mol/L acetic acid, and the mixture was processed using ultrasonic treatment for 2 h at normal temperature. After a period of static conditions, the supernatant liquid was centrifuged, and the supernatant was filtered through a 0.22- $\mu\text{m}$  membrane. Finally, the pH was adjusted to 4.5 by the addition of sodium acetate buffer solution.

Bi/RGO-MWNT-AuNP/SPE and flame atomic absorption spectrometry (FAAS) were employed separately to measure the Cd(II) and Pb(II) in the extract solutions of soil. Then, the extract solutions were spiked with different Cd(II) and Pb(II) concentrations and measured by Bi/RGO-MWNT-AuNP/SPE again. The results were shown in Table 3. It can be seen that the recovery of Cd(II) and Pb(II) were ranging from 91.98% to 105.36%, which can meet the requirement of rapid detection on-site.

**Table 3 Results for the Cd(II) and Pb(II) detection in soil samples**

Sample	Add	Bi/RGO-MWNT-AuNP/ SPE/mg kg <sup>-1</sup>		FAAS /mg kg <sup>-1</sup>		Recovery/%	
		Cd(II)	Pb(II)	Cd(II)	Pb(II)	Cd(II)	Pb(II)
1	-	1.57 $\pm$ 0.14	17.78 $\pm$ 0.84	1.49	16.92	105.36	105.08
	20	22.03 $\pm$ 0.51	38.12 $\pm$ 1.45			102.51	103.25
2	-	2.35 $\pm$ 0.24	23.49 $\pm$ 1.72	2.55	23.98	92.15	97.95
	20	22.95 $\pm$ 0.72	43.59 $\pm$ 2.65			101.77	99.11
3	-	1.95 $\pm$ 0.27	20.45 $\pm$ 1.85	2.12	19.56	91.98	104.55
	20	22.15 $\pm$ 0.83	41.45 $\pm$ 3.67			100.13	104.77

## 4 Conclusions

In summary, a nano-composite material was synthesized by GO, MWNT, and AuNP, which exhibits unique structural features. The electrochemical characteristics were improved significantly when bare SPE was modified with this new composite material. The RGO-MWNT-AuNP/SPE electroplated the Bi film ex-situ can detect Cd(II) and Pb(II) simultaneously with high sensitivity. This prepared electrode has shown excellent anti-interference and can be employed to measure field sample with high accuracy.

## Acknowledgements

This work was supported by the International Research Exchange Scheme of the Marie Curie Program of the 7th Framework Program (Ref. PIRSES-GA-2013-612659), Chinese National Natural Science Foundation (No. 31671578), the Fundamental Research Funds for the Central Universities (Grant No. 2016 XD001) and the Shandong Provincial Natural Science Foundation of China (No. ZR2015CM016).

## [References]

- [1] Li Z Y, Ma Z W, van der Kuijp T J, Yuan Z W, Huang L. A review of soil heavy metal pollution from mines in China: pollution and health risk assessment. *Science of the Total Environment*, 2014; 468-469: 843-853.
- [2] Zhou X, Zhu G, Sun J, Cailin Q. Toxicity of copper, zinc, lead, cadmium to tissue's cellurdna of the fish (*Carassius auratus*). *Acta Agriculturae Sinica*, 2001; 15: 167-173. doi: 10.1007/bf02141899.
- [3] Akcay H, Oguz A, Karapire C. Study of heavy metal pollution and speciation in Buyak Menderes and Gediz river sediments. *Water Research*, 2003; 37: 813-822. doi: 10.1016/s0043-1354(02)00392-5.
- [4] Duruibe J O, Ogwuegbu M O C. Heavy metal pollution and human biotoxic effects. *International Journal of Physical Sciences*, 2007; 2: 112-118. doi: 10.1163/2210-7975\_hrd-0514-0058.
- [5] Bala A, Suleiman N, Junaidu A U, Saliyu M D, Ifende V I, Saulawa M A, et al. Detection of lead (Pb), cadmium (Cd), chromium (Cr) nickel (Ni) and magnesium residue in kidney and liver of slaughtered cattle in Sokoto central abattoir, Sokoto state, Nigeria. *International Journal of Livestock Research*, 2014; 4: 74. doi: 10.5455/ijlr.20131002072458.
- [6] Cheng S. Heavy metal pollution in China: origin, pattern and control. *Environmental Science & Pollution Research International*, 2003; 10: 192-198.
- [7] Liu F F. Determination with graphite furnace atomic absorption spectrometry of lead content in pork. *Chinese Journal of Urban & Rural Enterprise Hygiene*, 2017. doi: 10.3403/02147605u.
- [8] Juanni N, Liu J, Zhang Y, Zhang P, Zhang H. Inductively Coupled Plasma Mass Spectrometry Lead, Cadmium in Drinking Water. *Guangdong Chemical Industry*, 2014. doi: 10.3403/30174177.
- [9] Li J X, Sun C J, Li Z, Jiang F H, Yin X F, Chen J H, et al. Determination of lead species in algae by capillary electrophoresis-inductively coupled plasma-mass spectrometry. *Chinese Journal of Analytical Chemistry*, 2016; 44: 1659-1664. doi: 10.1007/978-1-4939-6403-1\_10.
- [10] Chen K L, Jiang S J, Chen Y L. Determining lead, cadmium and mercury in cosmetics using sweeping via dynamic chelation by capillary electrophoresis. *Analytical & Bioanalytical Chemistry*, 2017; 409: 2461-2469. doi: 10.1007/s00216-017-0193-1.
- [11] Li Y N, Xu Z B, Liu S L. Determination of lead and arsenic in iron ore by X-ray fluorescence spectrometry based on genetic neural network. *Metallurgical Analysis*, 2017. doi: 10.13228/j.bouyan.issn1000-7571.010103
- [12] Zhang H, Jiang B, Xiang Y, Su J, Chai Y, Yuan R. DNAzyme-based highly sensitive electronic detection of lead via quantum dot-assembled amplification labels. *Biosensors & Bioelectronics*, 2011; 28: 135. doi: 10.1016/j.bios.2011.07.009.
- [13] Gumpu M B, Sethuraman S, Krishnan U M, Rayappan J B B. A review on detection of heavy metal ions in water-An electrochemical approach. *Sensors & Actuators B Chemical*, 2015; 213: 515-533. doi: 10.1016/j.snb.2015.02.122.
- [14] Mar í-Hormigos R, Gismera M J, Procopio J R, Sevilla M T. Disposable screen-printed electrode modified with bismuth-PSS composites as high sensitive sensor for cadmium and lead determination. *Journal of Electroanalytical Chemistry*, 2016; 767: 114-122. doi: 10.1016/j.jelechem.2016.02.025.
- [15] Abdi M M, Abdullah L C, Sadrolhosseini A R, Mat Yunus W M, Moxsin M M, Tahir P M. Surface plasmon resonance sensing detection of mercury and lead ions based on conducting polymer composite. *Plos One*, 2011; 6: e24578. doi: 10.1371/journal.pone.0024578.
- [16] López-García I, Vicente-Martínez Y, Hernández-Córdoba M. Determination of lead and cadmium using an ionic liquid and dispersive liquid-liquid microextraction followed by electrothermal atomic absorption spectrometry. *Talanta*, 2013; 110: 46-52. doi: 10.1016/j.talanta.2013.02.015.

- [17] Li T, Dong S, Wang E. A lead(II)-driven DNA molecular device for turn-on fluorescence detection of lead(II) ion with high selectivity and sensitivity. *Journal of the American Chemical Society*, 2010; 132: 13156. doi: 10.1021/ja105849m.
- [18] Rafiee M A. Graphene. *Dissertations & Theses - Gradworks*, 2011; 442: 282–286.
- [19] Khabashesku V N, Margrave J L. Chemistry of carbon nanotubes. *Cheminform*, 2006; 106: 1105–1136. doi: 10.5772/51869.
- [20] Sui Z, Meng Q, Zhang X, Ma R, Cao B. Green synthesis of carbon nanotube–graphene hybrid aerogels and their use as versatile agents for water purification. *Journal of Materials Chemistry*, 2012; 22: 8767–8771. doi: 10.1039/c2jm00055e.
- [21] Palanisamy S, Cheemalapati S, Chen S M. Amperometric glucose biosensor based on glucose oxidase dispersed in multiwalled carbon nanotubes/graphene oxide hybrid biocomposite. *Materials Science & Engineering C Materials for Biological Applications*, 2014; 34: 207–213. doi: 10.1016/j.msec.2013.09.011.
- [22] Dreyer D R, Park S, Bielawski C W, Ruoff R S. The chemistry of graphene oxide. *Chemical Society reviews*, 2014; 43: 5288. doi: 10.1039/b917103g.
- [23] Wang, Q, Wang, S, Shang, J, Qiu, S, Zhang, W, Wu, X, Li J H, Chen W X, Wang, X. Enhanced electronic communication and electrochemical sensitivity benefiting from the cooperation of quadruple hydrogen bonding and  $\pi$ - $\pi$  Interactions in graphene/multi-walled carbon nanotube hybrids. *ACS applied materials & interfaces*, 2017; 9(7): 6255–6264. doi: 10.1021/acsami.6b11157.
- [24] Verma H N, Singh P, Chavan R M. Gold nanoparticle: synthesis and characterization. *Veterinary World*, 2014; 7: 72–77. doi: 10.14202/vetworld.2014.72-77.
- [25] Xiao L L, Xu H B, Zhou S H, Song T, Wang H H, Li S Z, et al. Simultaneous detection of Cd(II) and Pb(II) by differential pulse anodic stripping voltammetry at a nitrogen-doped microporous carbon/Nafion/bismuth-film electrode. *Electrochimica Acta*, 2014; 143: 143–151. doi: 10.1016/j.electacta.2014.08.021.
- [26] Liu R, Cao H, Nie Z, Si S, Zhao X, Zeng X. A disposable expanded graphite paper electrode with self-doped sulfonated polyaniline/antimony for stripping voltammetric determination of trace Cd and Pb. *Analytical Methods*, 2016; 8: 1618–1625. doi: 10.1039/c5ay03094c.
- [27] Zhou H, Hou H, Dai L, Li Y, Zhu J, Wang L. Preparation of dendritic bismuth film electrodes and their application for detection of trace Pb(II) and Cd(II). *Chinese Journal of Chemical Engineering*, 2016; 24: 410–414. doi: 10.1016/j.cjche.2015.08.012.
- [28] Wang H, Zhao G, Zhang Z H, Yi Y, Wang Z Q, Liu G. A portable electrochemical workstation using disposable screen-printed carbon electrode decorated with multiwall carbon nanotube-ionic liquid and bismuth film for Cd(II) and Pb(II) determination. *International Journal of Electrochemical Science*, 2017; 12: 4702–4713. doi: 10.20964/2017.06.73.
- [29] Chaiyo S, Mehmeti E, K Ž, Siangproh W, Chailapakul O, Kalcher K. Electrochemical sensors for the simultaneous determination of zinc, cadmium and lead using a Nafion/ionic liquid/graphene composite modified screen-printed carbon electrode. *Analytica Chimica Acta*, 2016; 918: 26–34. doi: 10.1016/j.aca.2016.03.026.
- [30] Liu X, Li Z, Ding R, Ren B, Li Y. A nanocarbon paste electrode modified with nitrogen-doped graphene for square wave anodic stripping voltammetric determination of trace lead and cadmium. *Microchimica Acta*, 2016; 183: 709–714. doi: 10.1007/s00604-015-1713-3.
- [31] Wang H, Zhao G, Yin Y, Wang Z, Liu G. Screen-printed electrode modified by bismuth / $\text{Fe}_3\text{O}_4$  nanoparticle/ionic liquid composite using internal standard normalization for accurate determination of Cd(II) in Soil. *Sensors*, 2017; 18(1): 6. doi: 10.3390/s18010006.